

Hierarchical self-assembly of a striped gyroid formed by threaded chiral mesoscale networks

Jacob J. K. Kirkensgaard^{a,1}, Myfanwy E. Evans^b, Liliana de Campo^c, and Stephen T. Hyde^{a,c}

^aNiels Bohr Institute, University of Copenhagen, 2100 Copenhagen, Denmark; ^bTheoretische Physik, Friedrich-Alexander Universität Erlangen-Nürnberg, Staudtstrasse 7B, 91058 Erlangen, Germany; and ^cDepartment of Applied Mathematics, Research School of Physical Sciences, Australian National University, Canberra, ACT 0200, Australia

Edited by Steve Granick, University of Illinois at Urbana-Champaign, Urbana, IL, and accepted by the Editorial Board December 5, 2013 (received for review September 3, 2013)

Numerical simulations reveal a family of hierarchical and chiral multicontinuous network structures self-assembled from a melt blend of Y-shaped ABC and ABD three-miktoarm star terpolymers, constrained to have equal-sized A/B and C/D chains, respectively. The C and D majority domains within these patterns form a pair of chiral enantiomeric gyroid labyrinths (srs nets) over a broad range of compositions. The minority A and B components together define a hyperbolic film whose midsurface follows the gyroid minimal surface. A second level of assembly is found within the film, with the minority components also forming labyrinthine domains whose geometry and topology changes systematically as a function of composition. These smaller labyrinths are well described by a family of patterns that tile the hyperbolic plane by regular degree-three trees mapped onto the gyroid. The labyrinths within the gyroid film are densely packed and contain either graphitic hdb nets (chicken wire) or srs nets, forming convoluted intergrowths of multiple nets. Furthermore, each net is ideally a single chiral enantiomer, induced by the gyroid architecture. However, the numerical simulations result in defect-ridden achiral patterns, containing domains of either hand, due to the achiral terpolymeric starting molecules. These mesostructures are among the most topologically complex morphologies identified to date and represent an example of hierarchical ordering within a hyperbolic pattern, a unique mode of soft-matter self-assembly.

chirality | liquid crystals | entanglement | hyperbolic tilings | miktoarm copolymers

Liquid crystals formed by molecular self-assembly provide fascinating examples of complicated space partitions in soft-matter science. Relatively complex examples are the bicontinuous mesostructures found ubiquitously in both natural and synthetic soft matter, including lipid–water systems and block copolymer melts, namely the double diamond (symmetry $Pn\bar{3}m$), the primitive ($Im\bar{3}m$), and, particularly, the gyroid ($Ia\bar{3}d$) mesophases. The structure of these mesophases can be described by a molecular membrane folded onto one of the three simplest triply periodic minimal surfaces (TPMS), namely the D, P, and G(yroid) surfaces, named by Schoen in the 1960s (1). From a 3D perspective, these structures are characterized by the nets describing the pair of mutually threaded labyrinths carved out of space by the convoluted hyperbolic architecture of the TPMS. For the gyroid, this is a racemic mixture of two chiral srs nets, one left- and the other right-handed [the three-letter nomenclature follows the Reticular Chemistry Structure Resource naming convention for 3D nets (2)]. This leads to an overall achiral structure when the two nets are chemically identical, which is the case in most experimentally identified gyroid liquid-crystal structures. One such structure recently reported is a gyroid assembly found in an ABC three-miktoarm star terpolymer melt (3). In this structure, the majority C component constitutes the two labyrinth nets while the A and B minority components together form the dividing membrane. Because of the connectivity of the star molecular architecture and because all components microphase separate, the A and B components

segregate on the dividing hyperbolic interface. This structure is an experimental indication of a unique mode of self-assembly, namely “hierarchical assembly of a hyperbolic pattern.” Complementing this finding and further motivating our work reported here, a recent simulation study by one of us (J.J.K.K.) explored self-assembly of blends of equal amounts of two distinct three-miktoarm stars, namely ABC and ABD three-miktoarm star terpolymers (Fig. 1). Both molecules were assigned equal molecular weights, and the proportions of the equal volume C (green) and D (yellow) chains relative to the equal A (red) and B (blue) chains were varied (4). Despite these severe compositional constraints, a number of unique four-colored mesophases were revealed. The most striking feature of the predicted phase behavior in this system was the presence of interesting patterns whose general features are reminiscent of the gyroid, albeit far more complex in both geometric and topological aspects. In the system reported here, two ordering regimes form. At the larger length scale, ordering induces a gyroid-like membrane, which is itself also spontaneously ordered at a smaller length scale, giving unique microdomain patterning due to the membrane confinement to a hyperbolic curved interface. Each of these patterns contain distinct numbers and types of interwoven 2D and 3D A and B domains forming nets of equal hand, immersed within the hyperbolic interface between an enantiomeric pair of C and D srs nets. These structures are spectacularly convoluted in 3D space and correspond to special members of a sequence of chiral cubic patterns that emerge by local striping of the gyroid membrane. We demonstrate how this is performed systematically by

Significance

Chirality and hierarchical ordering are two fundamental properties found in many of nature’s most complex self-assembled structures such as living cells. Simultaneous control over these properties in synthetic systems is vital to mimic or even surpass nature’s designs. Via numerical simulations, we describe a class of complex morphologies that afford radically new architectures for self-assembled shapes. Specifically, a mixture of two star block-copolymers are shown to form multiple interwoven 2D and 3D labyrinths—all chiral—and hierarchically ordered on two different length scales. Furthermore, we show that such intricate network morphologies forming at a confined, hyperbolic interface can be classified and modeled in terms of a much simpler isotropic model of packing based on tilings of the hyperbolic plane.

Author contributions: J.J.K.K., M.E.E., L.d.C., and S.T.H. designed research; J.J.K.K., M.E.E., L.d.C., and S.T.H. performed research; J.J.K.K., M.E.E., L.d.C., and S.T.H. analyzed data; and J.J.K.K., M.E.E., L.d.C., and S.T.H. wrote the paper.

The authors declare no conflict of interest.

This article is a PNAS Direct Submission. S.G. is a guest editor invited by the Editorial Board.

¹To whom correspondence should be addressed. E-mail: jjkk@nbi.dk.

This article contains supporting information online at www.pnas.org/lookup/suppl/doi:10.1073/pnas.1316348111/-DCSupplemental.

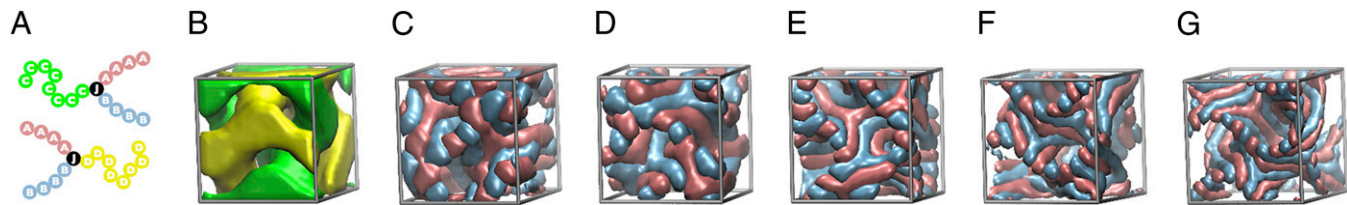


Fig. 1. (A) Model ABC and ABD three-miktoarm star terpolymer molecules. All molecules contain equal-sized A (red) and B (blue) arms, and longer C (green) and D (yellow) arms, also of equal size. The parameter x (equal to $8/4=2$ in this image), corresponds to the number ratio of C to A beads. (B) C and D domain geometry, a pair of intertwined srs nets. (C–G) Single-unit cell snapshots illustrating the curved striped pattern formed by the minority components A and B for varying x . (C) $x = 2$, (D) $x = 3.33$, (E) $x = 3.67$, (F) $x = 5$, and (G) $x = 6$. Note the threefold branching of the stripes for all values of x .

mapping a particular family of tilings in the hyperbolic plane onto the gyroid in 3D euclidean space. Careful analysis of the morphologies formed in the simulations, described below, reveals the presence of up to three distinct chiral cubic mesophases within this striped gyroid region of the phase diagram. We explore the geometric and topological variety of these self-assemblies in detail and discuss how they emerge as a response to a hierarchy of frustrations imposed by the three-arm star molecular architecture, acting in both two and three dimensions.

Molecular Simulations

ABC and ABD star molecules are constructed by linking three (distinctly colored) arms to a central junction bead. Each arm contains strings of beads whose lengths are tuned appropriately to form ABC and ABD stars whose number ratios are $1:1:x$, as shown in Fig. 1A. Interactions within and between molecules are governed by potentials that induce segregation of unlike colored beads. The simulation setup (described in more detail in *SI Text*) has previously been used to successfully predict complex self-assembly behavior in related polymer systems (4–8). A series of typical simulated mesostructures formed by these molecules is illustrated in Fig. 1C–G for different values of the composition parameter x defined in Fig. 1A. Despite the structural complexity of these four-colored patterns, they display spatial order and some degree of symmetry, apparent on visual inspection. For $x < 1.75$, four-colored columnar phases appear, and for $x > 7$, a hierarchical lamellar pattern is predicted (4). Over the window of compositions with x between 1.75 and 7, a variety of more complex morphologies consistently emerge. The two majority components (green C and yellow D) of the star molecules self-assemble to form segregated three-periodic domains consisting of an enantiomeric pair of interwoven labyrinths, whose channels lie on edges of left- and right-handed srs nets, as shown in Fig. 1B. Those labyrinths are separated by a gyroid-like film, containing the domains formed by the terpolymers' minor components (blue A and red B). Unlike conventional bicontinuous gyroid mesophases (9), the C–D net pair is composed of distinct chemical moieties, so the (colored) pattern is chiral, with space group symmetry $I4_{1}32$ analogous to the alternating gyroid found in linear ABC terpolymer melts. The identification of the simulated patterns with the gyroid is supported by structure factor calculations of the C and D domain coordinates within the cubic volume. The C and D domains yield identical spectra displaying a series of peaks consistent with those expected from srs nets with space group symmetry $I4_{1}32$ as shown in *SI Text*. More detailed quantitative analysis of the geometries can be done using various radial distribution functions (RDFs) calculated from the coordinates of the simulated patterns. This analysis is described in detail in *SI Text*. On the basis of these crystallographic and geometric arguments, we conclude that the star-molecular assemblies form AB bilayers, composed of a pair of back-to-back AB monolayers of constant thickness facing both sides of the gyroid (and the C and D domains). As this overall gyroid structure is a feature of all of the structures described

here, in the following we will focus on the AB film separating the C and D channels.

As can be seen in Fig. 1C–G, the simulations also clearly reveal segregation of the minor A and B components within the gyroid film that separates the C and D labyrinths. The A and B domains typically form multiple stripes around the channels of the gyroid, and their multiplicity around each channel varies with x . Furthermore, individual stripes regularly branch at threefold junctions, as seen in Fig. 1C–G and both A and B domains typically extend indefinitely over the curved gyroid film. The A–A RDFs are indistinguishable from the B–B RDFs (*SI Text*), indicating that the A and B domains are structurally identical. The simulated morphologies therefore consist of a pair of congruent (with inversion) 3D C and D labyrinths, separated by multiple congruent condensed A and B domains. The A and B domains are well described by reticulations of the gyroid with two-colored versions of regular, dense hyperbolic forests of degree three and related branched-ribbon tilings (10–13), described next.

Hyperbolic Forests on the Gyroid

Just as the euclidean plane can be tiled (or striped) by infinite parallel ribbons, the hyperbolic plane (\mathbb{H}^2) can be tiled with “ribbons” or tree-shaped “branched ribbons,” (Fig. 2A and B). However, the wealth of 2D hyperbolic tessellations far outstrips planar examples. Identification of tilings relevant to the striped gyroid structures requires some familiarity with hyperbolic geometry and symmetry. In particular, the exotic parallelism of hyperbolic space allows the reticulation of \mathbb{H}^2 with arrays of trees (i.e., infinite graphs without cycles), provided their edges are sufficiently long (11). “Regular” trees, with symmetrically equivalent edges and vertices (of any degree or branching order exceeding one), can be embedded in \mathbb{H}^2 such that symmetry operations exchange edges and vertices. Those isometries can be used to build infinite arrays of regular trees that reticulate \mathbb{H}^2 . Because the disjoint trees are close-packed in \mathbb{H}^2 , we call such reticulations “regular, dense forests” (11). These forests also define 2D “free” tilings of \mathbb{H}^2 that are unbounded in at least one direction, as illustrated in Fig. 2A and B. These are analogous to tilings of the euclidean plane by infinite parallel strip-like ribbons.

Free tilings of \mathbb{H}^2 can be mapped onto the gyroid, forming free tilings on the TPMS. This mapping necessarily involves some distortion compared with the perfectly homogeneous geometry of \mathbb{H}^2 , due to the curvature anisotropy of the gyroid compared with \mathbb{H}^2 . An unlimited number of tilings can be realized, whose homogeneity varies, breaking the degeneracy of these patterns in \mathbb{H}^2 . Among those tilings, regular free tilings most closely mimic the free tilings on \mathbb{H}^2 because they are realized on the gyroid with maximal symmetry, forming quasihomogeneous tiles. These maximally symmetric free tilings are formed by regular, dense forests. Regular, dense forests with threefold, fourfold, and sixfold vertices, composed of degree-three, -four, and -six trees, respectively, have been constructed on the gyroid TPMS (10–12). These forests, composed of degree- k trees, have orbifold symmetries $*222k$, $2*2k$, and $222k$, where $k = 3, 4, 6$. [Here, we adopt Conway's

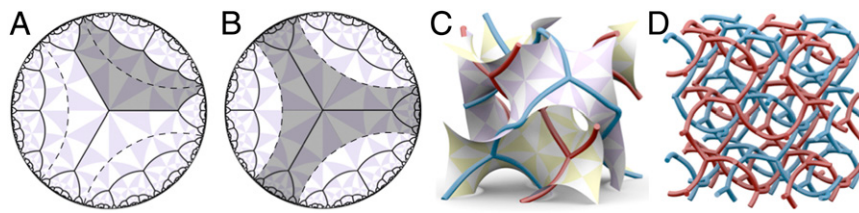


Fig. 2. Geometric modeling of close-packed degree-three forests. (A and B) Reticulation of \mathbb{H}^2 by a regular, dense forest with edge length $\cosh^{-1}(3)$ (full lines) and the separating geodesics (dashed lines) that define tilings of the hyperbolic plane: (A) A single infinite tile of a ribbon tiling. (B) A single infinite tile of a branched ribbon tiling whose spine is a single degree-three tree. The hyperbolic plane is drawn in the Poincaré disk model and decorated by triangular tiles. (C) Mapping of the spines of a two-colored branched ribbon reticulation onto a unit cell of the gyroid. (D) The resulting 3D nets upon removal of the gyroid surface: a pair of interwoven chiral **srs** nets of like hand.

orbifold notation (14).] The $k = 3$ solutions are particularly elegant: the threefold vertices occupy the least curved flat points on the gyroid (with threefold site symmetry), linked by edges into disjoint trees in various ways. Further details can be found in *SI Text* and elsewhere (10–13). We discuss below the relative stabilities of various regular degree-three patterns and resulting stripe geometries, which depend on extrinsic features of these forests.

Striped patterns, like those observed in the simulations, can be formed by coloring adjacent branched-ribbon tiles alternately red and blue. Because the edges of branched-ribbon tiles are vertex-free, and all edges bound two adjacent tiles, two coloring is possible for all branched-ribbon tilings. In contrast, ribbon tilings contain vertices, where more than two domains meet. This feature is incompatible with two coloring, because alternately coloring domains around a common vertex will result in fusion of domains at the vertex (and along common edges when the tiling is derived from degree- k forest where k is odd). Because the stripes seen in the simulations invariably contain threefold branches, relevant branched-ribbon tilings must be found among forests of degree three. It turns out that branched-ribbon tilings whose central spines are regular, dense hyperbolic forests of degree three—the most symmetric possible degree-three stripings of the gyroid—describe the principal features of the striped gyroid patterns observed in our simulations.

An unlimited number of these regular, dense, degree-three forests can be constructed geometrically from decorations of 2D orbifolds that cover the gyroid. The orbifolds $*2223$ and 2^*23 each yield a single dense, regular forest of degree three; the 2223 orbifold gives rise to a two-parameter family of forests (10, 12). Furthermore, all 2223 examples lead to two distinct branched-ribbon tilings on the gyroid, due to the pair of covering maps to the gyroid for \mathbb{H}^2 for all forests in this class (15) (see *SI Text*).

The most symmetric forest ($*2223$) has hyperbolic edges of length $\cosh^{-1}(3)$ (measured in \mathbb{H}^2). It is illustrated in Fig. 2B along with its corresponding branched-ribbon tiling. That forest, whose edges are the shortest of all regular, dense forests, maps onto the gyroid to form a pair of disjoint but mutually threaded curvilinear nets, whose edges run between neighboring flat points of the gyroid (Fig. 2C). The resulting 3D pattern is an interwoven pair of identical chiral nets, with curved edges, illustrated in Fig. 2D. Each net has the topology of the **srs** net (16). Other regular, dense forests with longer edges can be built that link successively more distant pairs of flat points. A series of structures within this family, with increasingly long edges, is shown in the top row of Fig. 3, labeled by their hyperbolic edge lengths. Recall that the labyrinths of the gyroid also describe an enantiomeric pair of interwoven **srs** nets; however, the pattern formed by the $\cosh^{-1}(3)$ forest on the gyroid is very different, because it contains mutually threaded, equivalent enantiomers.

All regular, dense forests on the gyroid necessarily form intergrowths of regular, crystalline nets (with symmetrically equivalent edges and vertices in both 2D hyperbolic and 3D Euclidean space). Only two embeddings of degree-three graphs in 3D Euclidean

space are regular: the 3-periodic **srs** net and the 2-periodic **hcb** pattern (17). With one exception, the regular degree-three forests explored here (shown in Fig. 3) form multiple threaded curvilinear chiral nets (of equal handedness) whose topologies are that of the **srs** net. The number of disjoint **srs** nets making up the gyroid film is either 2 or 54, as listed in *SI Text*, and each member has a distinct mode of net entanglement (11, 12). The forest with edge length $\cosh^{-1}(15)$ maps onto the gyroid to form chiral arrays of warped, mutually threaded **hcb** patterns, oriented perpendicular to the four (111) directions of the gyroid unit cell.

All of these patterns embed in 3D space to form chiral cubic structures, with space groups $P4_132$ (or $P4_332$ for the other enantiomer) or $I2_13$. Identification of each distinct pattern is, however, difficult from usual crystallographic considerations due to structural defects in the minority domains of the simulated patterns. However, a useful fingerprint of the various regular forests emerges from the distinct windings of the forest edges around channels of the gyroid. The number of edges packed around a channel (the stripe number) is dependent on the edge length, or forest type, providing a fingerprint for each regular pattern. (In technical terms, the construction is related to the homotopic class of the tree embeddings on the TPMS for each forest). Due to the symmetry of degree-three regular forests, the edge wrappings onto the gyroid fall into two distinct classes for each forest, with different stripe numbers around the channels of either class. A signature of ideal, defect-free regular forests consists of the pair of numbers, corresponding to the stripe numbers wrapping around each channel class. They are listed for

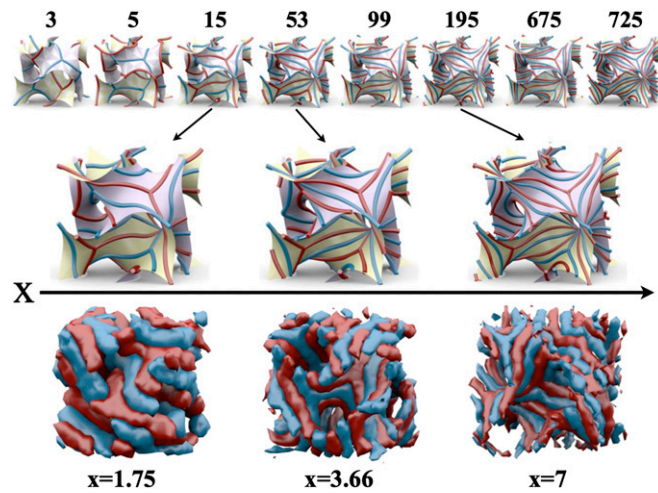


Fig. 3. (Top) A range of regular, dense degree-three forests on the gyroid, labeled by integers y , denoting forests with edges of length $\cosh^{-1}(y)$. (Middle) The subset of three forests that match most closely simulated morphologies. (Bottom)

the simpler regular degree-three forests in *SI Text*. Given that a pair of stripe numbers is characteristic of any such tiling, these data afford robust identification of the underlying tiling generated in these simulations, in the absence of structural defects.

To identify the relevant tilings, we have estimated stripe numbers by counting the number of distinct red and blue stripes winding around channels of the gyroid in the simulated structures (Fig. 4). Because the patterns contain defects (to be discussed in more detail below), the counts are statistical in nature (presented in full in *SI Text*). In some cases, domain branching in the vicinity of the channels, due to the presence of defects, does not allow definitive counts. However, despite that uncertainty, the data are consistent with three—and only three—of the signatures belonging to the degree-three branched-ribbon tilings. Those forests are the degree-three regular forests with edge lengths $\cosh^{-1}(15)$, $\cosh^{-1}(53)$, and $\cosh^{-1}(195)$, all from the same member of the pair of covering maps. Note that a pair of stripe numbers characterizes each forest, marked in Fig. 4. Individual stripe numbers occasionally diverge from the values expected from these three forests, but the pairs of numbers are consistent with those cases only, as shown in Fig. 4. These statistics do not allow us to firmly conclude whether transitions between these three forests are first or second order. However, the quasicontinuous nature of the plots as a function of x lead us to tentatively conclude that transitions between the distinct forests may be thermodynamically of second order, mediated by topological defects whose precise forms remain unclear.

In addition to the likely presence of topological defects within the generic patterns found in our simulations, geometric defects due to the inherent chirality of these patterns are found, which induce deviations of domains from the ideal **srs** topology. This is because the covering map from \mathbb{H}^2 to the gyroid can realize either left- or right-handed patterns. The degree-three forests reticulate the gyroid in two distinct orientations, related by rotations about the surface normal vector through any flat point by $\frac{\pi}{3}$. (Examples of both reticulations are shown in Fig. 5 and in *SI Text*.) Given that the star terpolymeric molecules in the copolymer simulations are achiral, left- and right-handed domains are equally stable in the self-assembled system. Indeed, patches of curvilinear **srs** or **hcb** nets of either enantiomeric form are

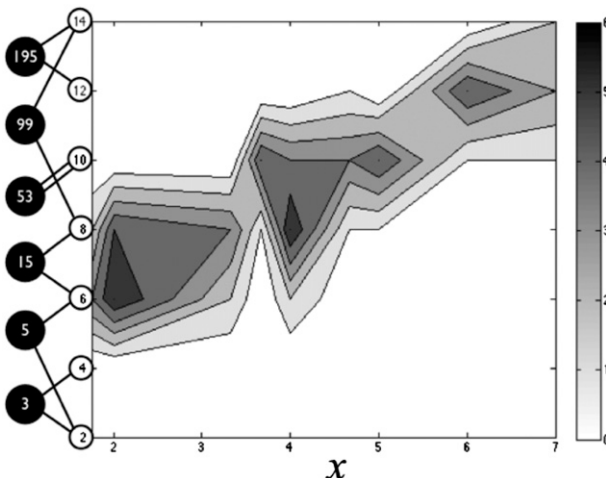


Fig. 4. Statistical variation of the number of A and B stripes packing around channels of the gyroid present in the simulated patterns as a function of the composition parameter x . The stripe numbers were counted around various channels of the unit cell (*SI Text*), and the intensity of the greyscale reflects the frequency of various stripe numbers. Compare data from tables in *SI Text*. The different forest and their pairs of stripe numbers are indicated on the Left.

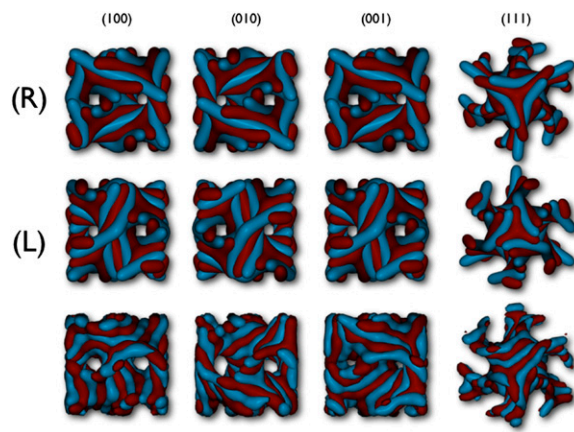


Fig. 5. Comparison of ideal left- (L) and right-handed (R) patterns from the regular forest with edge length $\cosh^{-1}(53)$ (top and middle rows) viewed from various directions with a self-assembled morphology formed in a simulated mixture of terpolymers with $x = 4$ (bottom row). Matches between the simulated morphologies and ideal left- and right-handed patterns are visible in distinct patches of the unit cell, which is therefore of mixed chirality.

visible at different locations, giving achiral patterns (Fig. 5). Structural defects associated with this feature likely account for some differences between the ideal regular forests and the simulated morphologies, including occasional variations in the stripe number statistics around channels, as well as small differences between simulated and ideal RDFs described below.

Given the presence of these defects, we have explored in more detail simulations for $x=4$, for which the stripe numbers are indicative of the $\cosh^{-1}(53)$ forest as the closest defect-free model. In Fig. 5, the ideal $\cosh^{-1}(53)$ forest and simulated structures are compared directly along different crystallographic directions. This structure is stable over a large range of simulation box sizes (see *SI Text*). RDFs for the correlations between junction beads in opposed monolayers reveal gradual and continuous small variations, suggesting continuous structural variations within a single “parent structure,” consistent with our hypothesis of second-order transitions between distinct forests. The identification of this parent structure as the defect-free $\cosh^{-1}(53)$ forest is further supported by comparison of these RDFs with those of a model structure, based on this regular forest (see details in *SI Text*). The calculations show excellent agreement between the simulation and model, as illustrated in Fig. 6. In summary, we conclude the following: The A and B domains form two-colored branched tilings on the gyroid, as illustrated schematically in Fig. 3. Three examples are found. Those three tilings are derived from the dense regular forests in \mathbb{H}^2 with edge lengths $\cosh^{-1}(15)$, $\cosh^{-1}(53)$, and $\cosh^{-1}(195)$ and are compared directly to simulation snapshots in Figs. 3 and 5. Defects that deform the patterns from those ideal geometries are also found, some of which may stabilize the patterns at intermediate concentrations, allowing second-order transitions between these forests.

Minimally Frustrated Striping of the Gyroid

The formation of these complex morphologies can be ascribed to the dominant driving forces for self-assembly of copolymer melts, namely the maximization of chain entropy of each constituent block and the minimization of interfacial surface tension, subject to the topological constraints of the star-shaped molecules. Because the interactions within each block are identical, and the number of beads of both minor blocks are matched, as are the bead numbers in both major blocks, the formation of geometrically equivalent C and D domains, as well as A and B domains, is

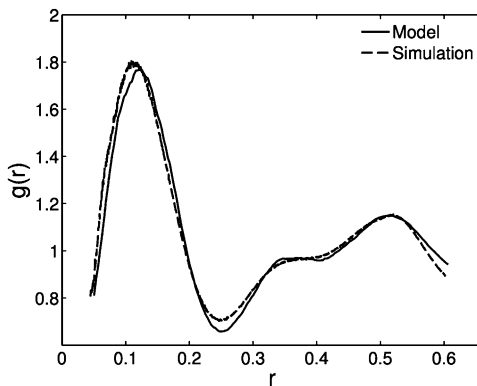


Fig. 6. RDFs from A–B bead correlation at $x = 4$ compared with model calculation based on ideal geometries with points lying on separating geodesics derived from the $\cosh^{-1}(53)$ tiling.

expected. Regular, dense forests on the gyroid offer an elegant spatial solution to this structural constraint.

These patterns are hierarchical self-assemblies, with two distinct length scales, resulting from two independent sources of geometrical frustration. The relative volumes of major and minor blocks enforce a curved interface between major and minor domains, and the formation of the gyroid-like interface can be explained by usual copolymer melt theory (e.g., ref. 18). The gyroid morphology emerges as the least frustrated embedding of a hyperbolic film with as far as possible constant (negative Gaussian) curvature and uniform labyrinth channel radii (19, 20). Segregation of A and B domains within the gyroid film is driven by the relative dimensions of the A and B blocks. These are equal, so equivalent domain morphologies are expected for each block. If those minority components were to self-assemble on a flat rather than a hyperbolic film, a lamellar pattern with alternating A and B ribbons would be expected. This is precisely what is found at slightly higher values of x where the formed morphology is a hierarchical lamellar structure (4). Unbranched striping is, however, impossible on the gyroid due to its nontrivial topology, and the presence of branches necessarily induces nonuniform stripe widths in the A and B domains. The relative energy of a branched ribbon can be estimated to lowest order from simple geometric considerations, outlined in *SI Text*. Those estimates show that threefold branched ribbons minimize the energetic cost associated with variations of ribbon width. We propose that the patterns form to minimize two independent sources of frustration, both associated with polymer chain packing. First, the gyroid forms, to minimize frustrations associated with the larger scale assembly, namely the (AB)–C and (AB)–D packing. Second, threefold branched stripes on the gyroid associated with regular, dense forests minimize the cost of variations in A and B stripe widths.

Given that these assemblies form dense regular forests on the gyroid, it is at first sight surprising that other forests, such as those with edge lengths $\cosh^{-1}(3)$, $\cosh^{-1}(5)$, and $\cosh^{-1}(99)$ are not observed in these simulations (Fig. 3). These other examples have very similar local geometry, but the theoretical stripe numbers listed in *SI Text* illustrates that they have very different configurations in 3D space. Indeed, the patterns found in the simulations are those with identical domain packings around both channel types [edge $\cosh^{-1}(53)$] or nearly so [edges $\cosh^{-1}(15)$ and $\cosh^{-1}(195)$], as seen in Fig. 4. This observation too can be explained by the tendency to form patterns whose ribbon width variations are minimized. Low-order branching affords minimal variations of widths along their length. However, differential geometric considerations imply that the variations in ribbon width from one side of the bilayer to the other depend on the direction of the ribbons with

respect to the principal directions in the gyroid (their tangential direction in the surface) (21). In general, stripes are thinner on one side of the gyroid than the other. Now the ribbon dimensions depend on their extrinsic orientation in the surface. If they align with principal directions, the ribbon laminae thin as one moves from the gyroid toward one labyrinth (e.g., C), and thicken to the other (D). However, if they follow the asymptotic directions on the surface, their width decreases symmetrically to both sides (21). The specific forests found in the simulations therefore result in nearly identical monolayer domains on either side of the gyroid, allowing the pair of AB monolayers to be realized with equivalent local molecular conformations. A useful measure of the deviations of tree edges from asymptotic directions is afforded by the pair of stripe numbers. If they are matched, the directions are asymptotic. Notice then that the forests that fit best our simulations are precisely those with matched or nearly matched stripe numbers (*SI Text*). We remark in passing that this constraint is a subtle one on the gyroid, due to the exotic extrinsic embedding of this minimal surface. In contrast, patterns formed on its related P and D minimal surfaces are more readily identified and will be discussed elsewhere.

Final Remarks

In summary, we find excellent agreement between simulations and a model of self-assembly of ABC and ABD star copolymers forming ABC and ABD monolayers molded to either side of the gyroid. The AB domains together form a gyroid film that separates the (right- and left-handed) **srs** labyrinths made of C and D domains. Sequestration of A and B beads within the film results in three distinct chiral, cubic branched-ribbon tilings of the gyroid, related to the mapping of regular, dense degree-three hyperbolic forests to the gyroid. Patches of both left- and right-handed morphologies are found in our simulations. The forests formed result in particularly equal dimensions in both A and B monolayer domains in three dimensions. Those dimensions are a result of the extrinsic embedding of hyperbolic patterns in 3D space via the gyroid.

The 3D structures of enantiomerically pure versions of these morphologies are extraordinarily complex. Two of the three distinct patterns—with edge lengths $\cosh^{-1}(53)$ and $\cosh^{-1}(195)$ —consist exclusively of interwoven **srs** nets, with either 2 or 54 like-handed **srs** nets alternating between A and B domains, immersed in a racemic pair of C and D **srs** domains. The third structure found in these simulations [with $\cosh^{-1}(15)$ edges] contains a racemic intergrowth of three-periodic **srs** C and D domains wound between four interwoven families of convoluted **hcb** (chicken-wire) nets, each containing either an A or B domain. Each family is oriented normal to a (111) direction. These intricate self-assemblies of liquid-like domains rival, and indeed in some respects mimic, the complex interwoven networks in synthetic metal-organic framework (MOF) molecular crystals (22). For example, a MOF containing a “record” intergrowth of 27 left- and 27 right-handed **srs** nets has been reported recently (23). That pattern is related to the chiral 54 **srs** structure described here. Despite these very convoluted 3D forms, the structures we report emerge as the optimal solutions to the problem of combining hyperbolic films—driven by asymmetry between larger C and D blocks compared with the A and B blocks—with in-film segregation into equal domains. The shapes that result are those that are most nearly homogeneous in 3D space, and their structural complexity is driven by inherent frustration at two levels: the curvature and packing frustration relieved by the formation of the gyroid, and the domain width frustration relieved by forming degree-three tilings around regular, dense forests. The resulting chiral multiply threaded patterns are spectacular; they are surely among the most complex self-assemblies identified to date.

An important question is whether these extraordinary mesostructured self-assemblies may also be realized in other (simpler)

molecular melts, for example containing only one species of ABC star terpolymers. There are no geometric or topological reasons to exclude their formation. However, it is well known from linear block copolymer systems that the phase windows for complex network morphologies are different in AB and ABC systems. For example, both the (alternating) gyroid and the *Fddd* (O^{70}) phase windows are significantly smaller in AB diblock melts (24–26) compared with linear ABC triblock melts. The rationale behind this is that the addition of an extra component disrupts the balance between entropic and enthalpic free energy contributions when the composition is also unbalanced (27, 28) as is the case in this context. We therefore expect the phase window to be smaller in a pure ABC star system compared with the ABC–ABD binary blend investigated here and as a result more difficult to locate in theory or experiments. Furthermore, even if formed, it is uncertain whether a pure ABC star melt would stabilize the striped gyroid over a sufficiently broad composition range to admit the structural polymorphism reported here for binary blends. However, our

simulations model a melt blend with no polydispersity, symmetric interaction parameters between blocks, and with a single chain of each species. Therefore, in practice, the rigid constraints imposed in this study can be relaxed, possibly effecting a broader region of existence even in a pure ABC melt. For example, adding extra arms of the different species is known to expand phase windows of curved structures in star copolymer systems (7, 29). Given current activity in exploring melts of miktoarm copolymers, we anticipate the discovery of these and related liquid crystalline phases in mesostructured materials in the near future.

ACKNOWLEDGMENTS. We thank Toen Castle for his contribution to the understanding of stripes traveling in the asymptotic directions on minimal surfaces. J.J.K.K. acknowledges financial support from The Lundbeck Foundation and UNIK Synthetic Biology. M.E.E. acknowledges support from the Alexander von Humboldt Foundation as well as the German Research Foundation (Deutsche Forschungsgemeinschaft) through the research group Geometry and Physics of Spatial Random Systems under Grant SCHR1148/3-1. J.J.K.K. and S.T.H. are grateful to GILT for support.

1. Schoen AH (1970) *Infinite Periodic Minimal Surfaces Without Self-Intersections* (National Aeronautics and Space Administration, Washington, DC), NASA Technical Report TN D-5541.
2. O'Keeffe M, Peskov MA, Ramsden SJ, Yaghi OM (2008) The Reticular Chemistry Structure Resource (RCSR) database of, and symbols for, crystal nets. *Acc Chem Res* 41(12):1782–1789.
3. Matsushita Y, Hayashida K, Dotera T, Takano A (2011) Kaleidoscopic morphologies from ABC star-shaped terpolymers. *J Phys Condens Matter* 23(28):284111.
4. Kirkensgaard JJK (2012) Kaleidoscopic tilings, networks and hierarchical structures in blends of 3-miktoarm star terpolymers. *Interface Focus* 2(5):602–607.
5. Kirkensgaard JJK (2010) Novel network morphologies and compositionally robust 3-colored perforated lamellar phase in $A(BC)_2$ miktoarm star copolymer melts. *Soft Matter* 6:6102–6108.
6. Kirkensgaard JJK (2011) Systematic progressions of core-shell polygon containing tiling patterns in melts of 2nd generation dendritic miktoarm star copolymers. *Soft Matter* 7:10756–10762.
7. Kirkensgaard JJK (2012) Striped networks and other hierarchical structures in $A_mB_mC_n$ ($2m+n$)-miktoarm star terpolymer melts. *Phys Rev E Stat Nonlin Soft Matter Phys* 85(3 Pt 1):031802.
8. Kirkensgaard JJK, Fragouli P, Hadjichristidis N, Mortensen K (2011) Perforated lamellae morphology in novel P2VP(PDMS-b-PI-PS)2 3-miktoarm star quarterpolymer. *Macromolecules* 44:575–582.
9. Hyde ST (1989) The microstructure of bicontinuous surfactant aggregates. *J Phys Chem* 93:1458–1464.
10. Evans ME, Robins V, Hyde ST (2013) Periodic entanglement II: Weavings from hyperbolic line patterns. *Acta Crystallogr A* 69(3):262–275.
11. Hyde ST, Oguey C (2000) From 2D hyperbolic forests to 3D Euclidean entangled thickets. *Eur Phys J B* 16:613–630.
12. Evans ME, Robins V, Hyde ST (2013) Periodic entanglement I: Networks from hyperbolic reticulations. *Acta Crystallogr A* 69(3):241–261.
13. Castle T, Evans ME, Hyde ST, Ramsden S, Robins V (2012) Trading spaces: Building three-dimensional nets from two-dimensional tilings. *Interface Focus* 2(5):555–566.
14. Conway JH, Burgiel H, Goodman-Strauss C (2008) *The Symmetries of Things* (A K Peters, Wellesley, MA).
15. Robins V, Ramsden S, Hyde ST (2005) A note on the two symmetry-preserving covering maps of the gyroid minimal surface. *Eur Phys J B* 48:107–111.
16. Ramsden SJ, Robins V, Hyde ST (2004) 2d hyperbolic tilings by infinite tiles. Available at http://epinet.anu.edu.au/infinite_tiles. Accessed December 28, 2013.
17. Delgado Friedrichs O, O'Keeffe M, Yaghi OM (2003) Three-periodic nets and tilings: Regular and quasiregular nets. *Acta Crystallogr A* 59(Pt 1):22–27.
18. Cochran EW, Garcia-Cervera CJ, Fredrickson GH (2006) Stability of the gyroid phase in diblock copolymers at strong segregation. *Macromolecules* 39:2449–2451.
19. Hyde ST, et al. (1997) *The Language of Shape* (Elsevier Science, Amsterdam).
20. Schroder-Turk GE, Fogden A, Hyde ST (2006) Bicontinuous geometries and molecular self-assembly: Comparison of local curvature and global packing variations in genus-three cubic, tetragonal and rhombohedral surfaces. *Eur Phys J B* 54:509–524.
21. Goetz A (1970) *Introduction to Differential Geometry* (Addison-Wesley, Reading, MA).
22. Carlucci L, Ciani G, Proserpio DM (2003) Polycatenation, polythreading and polyknitting in coordination network chemistry. *Coord Chem Rev* 246:247–289.
23. Wu H, Yang J, Su Z, Batten SR, Ma J (2011) An exceptional 54-fold interpenetrated coordination polymer with 10^3 -srs network topology. *J Am Chem Soc* 133:11406–11409.
24. Meuler AJ, Hillmyer MA, Bates FS (2009) Ordered network mesostructures in block polymer materials. *Macromolecules* 42:7221–7250.
25. Matsen MW (1998) Gyroid versus double-diamond in ABC triblock copolymer melts. *J Chem Phys* 108:785–796.
26. Guo Z, et al. (2008) Discovering ordered phases of block copolymers: New results from a generic Fourier-space approach. *Phys Rev Lett* 101(2):028301.
27. Matsen MW, Thompson RB (1999) Equilibrium behavior of symmetric ABA triblock copolymer melts. *J Chem Phys* 111:7139–7146.
28. Bates FS (2005) Network phases in block copolymer melts. *MRS Bull* 30:525–532.
29. Matsen MW, Schick M (1994) Microphase separation in starblock copolymer melts. *Macromolecules* 27:6761–6767.